CHEMPHYSCHEM

DOI: 10.1002/cphc.201000452

In situ X-ray Absorption Analysis of ~1.8 nm Dendrimer-Encapsulated Pt Nanoparticles during Electrochemical CO Oxidation

Michael G. Weir,[a] V. Sue Myers,[a] Anatoly I. Frenkel,*[b] and Richard M. Crooks*[a]

We report an in situ X-ray absorption-fine structure (XAFS) spectroscopic analysis of ~1.8 nm Pt dendrimer-encapsulated nanoparticles (DENs) during electrocatalytic oxidation of CO. The results indicate that Pt nanoparticles encapsulated within poly(amidoamine) (PAMAM) dendrimers and immobilized on a carbon electrode retain their electrocatalytic activity and are structurally stable for extended periods during CO oxidation. This is a significant finding, because nanoparticles in this size range are good experimental models for comparison to first-principles calculations if they remain stable.

1. Introduction

Herein, we report an in situ X-ray absorption-fine structure (XAFS) spectroscopic analysis of ~1.8 nm Pt dendrimer-encapsulated nanoparticles (DENs) during electrocatalytic oxidation of CO. These results represent a significant advance in understanding the structure and stability of very small nanoparticles under catalytic conditions. Specifically, the data indicate that Pt nanoparticles encapsulated within poly(amidoamine) (PAMAM) dendrimers retain their electrocatalytic activity and are structurally stable for extended periods during CO oxidation. This is important, because Pt DENs, and DENs in general, are a good experimental model for studying catalytic reactions at nanoparticles containing 40–240 atoms. This is the interesting size range in which nanomaterials undergo rapid transitions in chemical and physical properties.[1] Moreover, the lower end of this range is compatible with first-principles calculations, and therefore there is an opportunity to directly compare theory to experimental results if the catalysts retain their structural integrity during the time required to make catalytic rate measurements.[2]

Pt DENs containing an average of 40–240 atoms have previously been prepared within fourth- and sixth-generation PAMAM dendrimers.[3] The synthesis involves two steps. First the Pt complex, $PtCl_4^{2-}$, undergoes hydrolysis, and then it reacts with interior tertiary amines of the dendrimer. Second, addition of $NaBH_4$ results in reduction of the coordinated Pt ions to atoms, which quickly coalesce into nanoparticles. We have recently shown that this synthesis yields a bimodal distribution of products: roughly half the dendrimers contain fully reduced Pt nanoparticles, and the other half contain unreduced Pt^{2+} (herein we denote all forms of unreduced platinum as Pt^{2+}, even though Pt^{2+} may be coordinated to the dendrimer, OH^-, Cl^-, or other species present in solution).[3b] Pt DENs, and alloys thereof, can be immobilized onto electrode surfaces and are active for the oxygen reduction reaction (ORR),[3d,e,4] CO oxidation,[3d] H^+ reduction,[3d] and H_2 oxidation.[3d] We have previously reported that the rate of the ORR is a sensitive function of catalyst size,[3d] and that the rate of the ORR at PtPd bimetallic DENs depends on the relative composition of the two metals.[4]

In addition to our own studies of Pt DENs, there have been numerous experimental and theoretical reports from other groups.[3a,5] For example, Miyahara and coworkers recently demonstrated that the reaction between interior tertiary amines of PAMAM dendrimers and Pt^{2+} is temperature dependent.[5 h] Amiridis and coworkers explored the platinum–dendrimer system using a slightly different synthetic technique that did not result in reduction of the precursor complex.[3a] Yamamoto et al. examined the electrocatalytic properties of Pt DENs for the ORR using a different type of dendrimer and reported exceptional catalytic activity for the smallest (~1 nm) nanoparticles.[6]

While the structural characteristics of DENs are beginning to emerge, very little is known about their properties during catalytic reactions. As mentioned earlier, our primary interest in DENs is in directly correlating first-principles theory to experimental catalytic rate measurements. For this purpose, it is essential that the structure of the catalyst remain unchanged (or at least that the changes be understood) in operando. As a first step toward understanding how DEN structure evolves

[a] M. G. Weir, V. S. Myers, Prof. R. M. Crooks
Department of Chemistry and Biochemistry
Texas Materials Institute
and
The Center for Nano- and Molecular Science and Technology
The University of Texas at Austin, 1 University Station
A5300, Austin, TX 78712-0165 (USA)
Fax:(+1) 512-425-8651
E-mail: crooks@cm.utexas.edu

[b] Prof. A. I. Frenkel
Department of Physics, Yeshiva University
245 Lexington Ave., New York, NY 10016 (USA)
Fax:(+1) 212-340-7868
E-mail: anatoly.frenkel@yu.edu

Supporting information for this article is available on the WWW under http://dx.doi.org/10.1002/cphc.201000452.

during catalysis, we examined the oxidation of CO to CO_2. This reaction has specific characteristics that make it appropriate for this study. First, the rate of this reaction is easily controlled via the electrode potential. Second, the intermediate species, adsorbed CO, can be retained on the electrode surface long enough to obtain XAFS spectra. Finally, this electrochemical reaction has been studied extensively both on single-crystal Pt and on nanoparticles, and therefore benchmarks exist for interpreting results.[7] For example, CO adsorption on Pt/Cu near-surface alloys results in a Cu-rich surface due to the enhanced strength of the Pt–CO bond in the presence of a Pt/Cu surface alloy.[8] Additionally, it has been shown that Pt nanoparticles agglomerate during CO adsorption and oxidation.[7c,9] Markovic and coworkers have used repeated potential cycling in a CO-rich solution to restructure the surface of Pt nanoparticles in their studies of particle-size effects.[7a,d] This group also found that adsorption of OH at surface defect sites affects the potential for CO oxidation.

Extended XAFS (EXAFS) provides information about the local environment of atoms in nanoparticles like DENs. This information includes the chemical identity, average bond lengths, and ensemble-average coordination number (CN) of atoms close to the x-ray absorbing atom.[10] X-ray absorption near-edge structure (XANES) contains information about the charge state of the absorbing atom, and therefore it is sensitive to the oxidation state of the absorber and its changes during in situ transformations. EXAFS and XANES data can both be collected in situ during electrochemical reactions, but for Pt nanoparticles smaller than ~5 nm in diameter, such studies have largely been confined to applications related to fuel cells.[11] These prior studies are distinguished from the results presented herein by the size and composition of the catalyst and its support. For example, Russell and coworkers studied the adsorption of CO to commercial, carbon-supported Pt catalysts ranging in size from 1–10 nm and reported sensitivity to surface adsorbates. Specifically, they were able to detect both CO and Pt oxides, and they could distinguish between Pt–CO and Pt–support interactions.[11h] Adzic and coworkers studied the ORR at core–shell particles consisting of Pt monolayers on nano-sized substrates including NbO_2.[11l] In these studies, the Pt interatomic distance could be controlled by changing the core material, and this in turn led to tuning of the catalytic activity.

Herein, Pt DENs containing an average of 240 atoms were encapsulated within sixth-generation, hydroxyl-terminated PAMAM dendrimers (G6-OH), and then immobilized onto carbon paper electrodes. The CNs were measured in electrolyte solution before and after application of an electrode potential, and before, during, and after CO adsorption. Two significant results emerge from this study. First, the Pt CN of the electrode-immobilized DENs increases significantly after the first application of a reducing potential and then it remains constant. This result is consistent with our previous study,[3b] and it suggests that the fraction of unreduced Pt DEN precursors originally present after BH_4^- reduction is converted to fully reduced DENs by the potential applied to the electrode. Second, CO adsorbs to Pt DENs and is then electrochemically oxidized to CO_2 without measurable change to the encapsulated nanoparticles. This is an important finding, because it means these DENs are dimensionally stable on the timescale of the XAFS measurements. Accordingly, the effect of DEN size and composition on catalytic reactions can be studied without fear of time-dependent agglomeration or other changes.

2. Results and Discussion

2.1. DENs Synthesis

Details regarding the synthesis of Pt DENs containing an average of 240 atoms [G6-OH(Pt_{240})] are provided in the Experimental Section and have been reported previously.[3b–e,4] Briefly, however, $PtCl_4^{2-}$ was allowed to complex with an aqueous solution of G6-OH for 72 h. The resulting precursor complex [G6-OH(Pt^{2+})$_{240}$] was then reduced with BH_4^-. UV/Vis spectra and TEM micrographs of the resulting DENs were consistent with previous reports and are provided in the Supporting Information (Figure S1). The DENs were purified by dialysis prior to electrochemical experiments.

2.2. Immobilization of DENs onto Glassy Carbon Electrodes (GCEs)

Figure 1a shows cyclic voltammograms (CVs) obtained during immobilization of Pt DENs to a GCE.[8] The immobilization procedure consists of cycling the potential of the GCE from −0.2 V to 0.7 V three times. The first scan has a slightly higher anodic current, beginning at ~0.4 V, compared to subsequent scans. We do not know how this observation correlates to the mechanism of DEN immobilization, but we have shown previously that it leads to a strong and irreversible link between the dendrimer and the GCE.[3d,e,4]

2.3. CO Oxidation

For comparison, CO oxidation experiments were performed on two different electrodes: bulk polycrystalline Pt and a DEN-modified GCE. Each electrode was immersed in a CO-saturated aqueous 0.1 M $HClO_4$ solution in the standard electrochemical cell (see the Experimental Section for the terminology used to identify the three different types of cells used herein) for 10 min at −0.7 V, and then the electrolyte solution was purged with N_2. It has previously been reported that this treatment results in chemisorption of a CO monolayer.[7a–c,9] Finally, the electrode potential was cycled twice from −0.7 to 0.8 V.

CVs for oxidation of CO on the polycrystalline Pt electrode are shown in Figure 1b. At the start of the first scan (red line, −0.7 V), the Pt surface is covered with CO and therefore no H-oxidation peaks are observed. As the electrode is scanned to more oxidizing potentials (0.10 V), adsorbed CO is oxidized to CO_2 and then desorbs from the surface. At the highest potentials, the increased current results from oxidation of the Pt surface. On the return sweep, a small amount of Pt oxide is reduced at ~0.0 V, followed by the reductive adsorption of H^+ onto the Pt surface. The second cycle has many of the same features as the first, but it also shows a H-desorption peak at

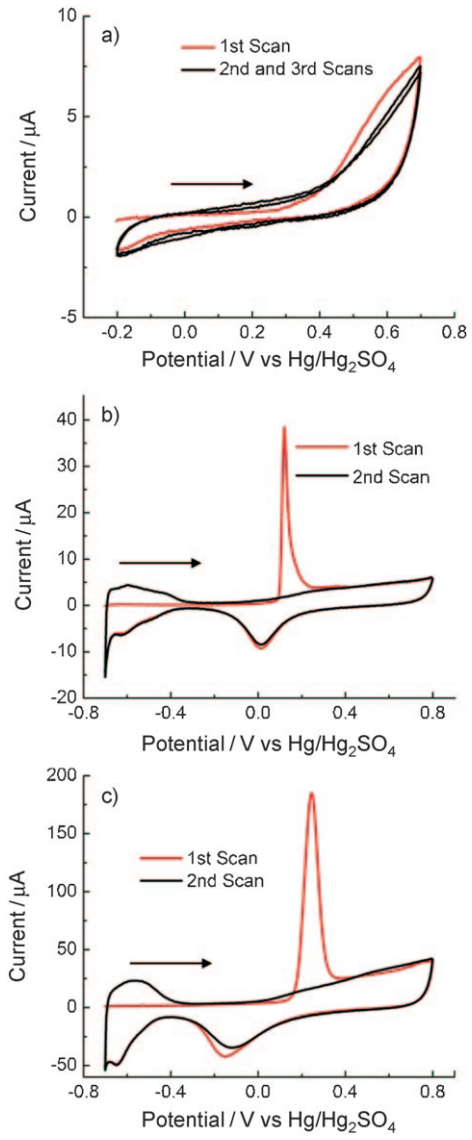

Figure 1. Cyclic voltammograms for a) the immobilization of G6-OH(Pt_{240}) DENs to a GCE, b) CO oxidation on a bulk, polycrystalline Pt electrode, and c) CO oxidation on the DEN-modified GCE. The immobilization (a) was performed at 10 mV s^{-1} in a dialyzed 10 μM solution of G6-OH(Pt_{240}) DENs with 0.1 M $LiClO_4$ as electrolyte. The CO oxidation experiments (b and c) were performed at 50 mV s^{-1} in 0.1 M $HClO_4$. These experiments were performed in the standard electrochemical cell (see text for details about the cells used herein).

~−0.6 V and no CO oxidation peak. All of these observations are in accord with literature reports.[7,12]

The oxidation of CO on the Pt DENs-modified GCE (Figure 1c) displays features similar to those just described for the polycrystalline Pt electrode. However, consistent with previous reports, the CO oxidation peak is both broader and at a more positive potential for the DENs.[3d] These observations are consistent with more heterogeneity in the CO binding sites for the DENs, compared to bulk Pt, and stronger adsorption of CO to the nanoparticles, respectively.[13] Similar findings have been reported for Pt nanoparticles in this size range prepared by other methods.[7a] The H-adsorption region extends to slightly less positive potentials for the Pt DENs, indicating that H^+ is harder to reduce on the DENs compared to a bulk Pt electrode. Additionally, for the polycrystalline Pt electrode there are smaller features atop the broader current envelope in this potential region, which arise from both hydrogen and anion adsorption and desorption from specific crystal faces.[14] Finally, the Pt oxide reduction wave for the DENs is displaced ~200 mV negative compared to the bulk Pt electrode.[15]

The areas under the CO oxidation peaks were integrated to estimate the total Pt surface area. As is customary for polycrystalline Pt surfaces,[7b] we assumed a charge-per-unit-area of 420 μC cm^{-2} for this calculation for both bulk Pt and Pt DENs. However, the corresponding value for Pt nanoparticles is unknown, and therefore the surface area estimate for the DENs must be considered within this context.[3d] The true surface area for the bulk Pt electrode, measured using the data in Figure 1b, is 0.069 cm^2, and its geometric area is 0.032 cm^2. The ratio of measured area to geometric area, or roughness factor, is, therefore, 2.15, which is consistent with previous reports.[16] The surface area of the Pt DENs, measured using the data in Figure 1c, is 0.57 cm^2. The surface area of the Pt DENs was estimated using several reasonable assumptions: a roughness factor of 2.4 for the GCE, one spherical nanoparticle per dendrimer, and a surface coverage of one dendrimer per 35 nm^2 of GCE surface area.[3d] This calculation yields an estimated Pt surface area of 0.049 cm^2. The difference between the measured (0.57 cm^2) and estimated (0.049 cm^2) areas by an order of magnitude is similar to, but higher than, that observed in previous studies of Pt DENs.[3d] We rationalize the difference in the ratios between this study and the previous report by considering the difference in electrode roughness and the electrode pretreatment.

2.4. Immobilization of DENs onto a Carbon Paper Electrode

G6-OH(Pt_{240}) DENs were immobilized onto a carbon paper electrode following a procedure reported by Godinez et al. and described in the Experimental Section.[17] Briefly, the hydrophobic carbon paper was rendered hydrophilic using an electrochemical pretreatment step in the Teflon cell. The carbon paper was then rinsed and immersed in a Pt DENs solution overnight, resulting in immobilization of the dendrimers. We speculate that oxygen-containing functional groups introduced onto the carbon surface by electrochemical cycling provide sites for hydrogen bonding or electrostatic adsorption of dendrimers.[5a,18]

Immobilization of Pt DENs onto the carbon paper was confirmed using cyclic voltammetry. Figure 2a compares CVs in the H-adsorption region for carbon cloth electrodes modified with empty G6-OH dendrimers and G6-OH(Pt_{240}) DENs. The CV for the empty dendrimers is featureless, except for a significant capacitive background, indicating an absence of catalytic activity. In contrast, the CV for the carbon paper electrode modified with Pt DENs exhibits significant catalytic activity for reduction of protons and subsequent oxidation of adsorbed H atoms. Additionally, there is a smaller feature at the extreme positive end of the scan range, which corresponds to formation of Pt oxide. These results confirm the presence of Pt DENs, and that

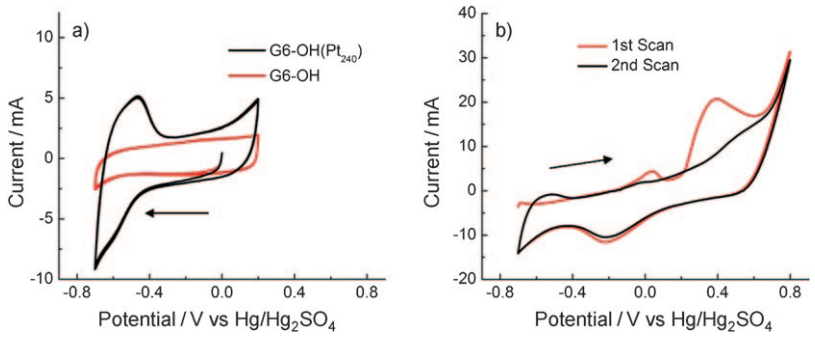

Figure 2. Cyclic voltammograms obtained in 0.1 M $HClO_4$ using a carbon paper working electrode. a) A scan of the hydrogen adsorption region using a G6-OH modified electrode (red line) and an electrode modified with G6-OH(Pt_{240}) DENs (black line) (scan rate = 50 mV s^{-1}). b) The first (red line) and second (black line) scans of the CO oxidation region (scan rate = 50 mV s^{-1}). These experiments were performed in the standard electrochemical cell.

the DENs are in electrical contact with the carbon paper working electrode.

The CV of the carbon paper modified with Pt DENs differs from the corresponding data for the GCE (Figure 1c, second scan) in that the former displays higher capacitance and a slightly sloped resistive background. These changes are ascribed to both the higher resistance of the carbon paper and its substantially higher surface area (~3.1 cm^2 geometric).

2.5. CO Oxidation on a Carbon Paper Electrode

Figure 2b shows a CV for CO oxidation on a Pt DEN-modified carbon paper electrode in the standard electrochemical cell. With the exception of the electrode materials, this experiment was performed using the same conditions described for the GCE (Figure 1c). The first scan in the positive direction displays the features anticipated by the results on the DEN-modified GCE: no H-oxidation (< −0.6 V), CO oxidation (~0.35 V), and Pt oxidation (> 0.6 V). However, these major features are shifted positive and broadened by the resistance of the carbon paper electrode compared to the GCE. The resistance of the cell is also observed as a sloping background current. In addition to the expected features, there is a small peak in this CV at 0.05 V. It may be associated with an interaction between the carbon paper and the Pt DENs, and we have observed that it varies in intensity with both batch and thickness of carbon paper.

Upon reversal of the positive-going scan, reduction of Pt oxide is observed at ~ −0.25 V, and there is a small peak for H adsorption at ~ −0.7 V. Note that the CVs shown in parts (a) and (b) of Figure 2 were performed on different samples, so some variation in both the H-adsorption peaks and the capacitive background are expected due to differences in Pt DENs loading.

There is a small Pt–H oxidation peak present at ~ −0.6 V in the second scan, but the CO oxidation peak is absent. These results are consistent with the data for the Pt DEN-modified GCE (Figure 1c). Note that the smaller anodic peak at 0.05 V is also not present in the second scan.

2.6. Electrochemistry

The in situ electrochemical XAFS experiments require a highly specialized cell geometry (Scheme 1). This cell design evolved as a compromise between the need to simultaneously optimize the electrochemical and spectroscopic measurements, and therefore it is not ideal for either. More details about the cell design are included in the Experimental Section. The XAFS cell and XAFS experiments required slight changes to

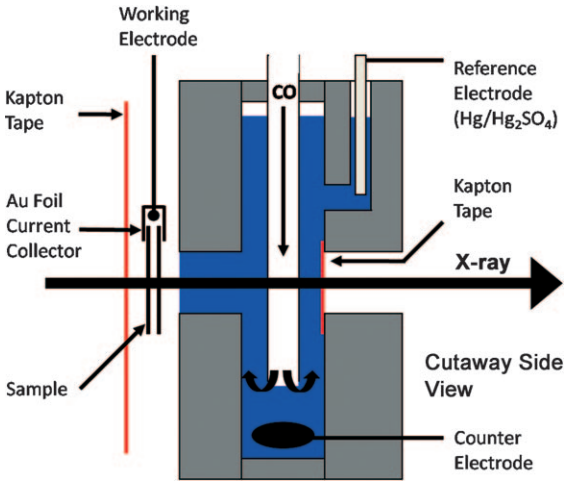

Scheme 1. Cell geometry for in situ electrochemical XAFS experiments.

the procedure described earlier for CO adsorption to the Pt DENs. First, instead of initially stepping the potential from open circuit to −0.7 V, as was done for the experiments shown in Figure 2b, the electrode potential was swept from −0.2 to −0.7 V at 50 mV s^{-1}, and then held at −0.7 V. This was necessary because of the high surface area of the electrode, and the corresponding need to maintain the maximum current passing through the cell below the limit defined by the potentiostat. In addition, to allow time for the XAFS spectra to be acquired, the potential was held at −0.7 V in the presence of CO for 4 h rather than 10 min.

The CV in Figure 3 shows the oxidation of CO in the XAFS cell. The electrochemical parameters used to obtain these data were identical to those described for Pt DENs on carbon paper in the smaller cell (Figure 2b). Note the prominent resistive background arising from the electrode material and cell geometry. The peaks in the CVs are also quite similar to those in Figure 2b, except they are broadened and shifted in potential (~0.4 V vs ~0.6 V for Figures 2b and 3, respectively). Importantly, each feature of the ideal CO oxidation exhibited by the Pt DENs on a GCE (Figure 1c) is observed.

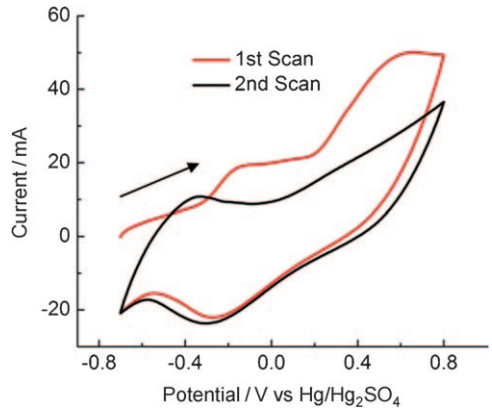

Figure 3. Cyclic voltammograms showing the first (red line) and second (black line) scans of the CO oxidation region for a G6-OH(Pt_{240}) DEN-modified carbon paper electrode using the in situ EXAFS cell. The scan rate was 50 mV s^{-1} and the electrolyte was 0.1 M $HClO_4$.

2.7. EXAFS Analysis

Figure 4 shows the *r*-space data and fits for the Pt L_3 edge for each in situ EXAFS experiment. The corresponding *k*-space data are provided in the Supporting Information (Figure S2). Parameters resulting from the fits, as well as the experimental conditions, are given in Table 1. Prior to sparging the solution with gas or placing the working electrode under potential control (Experiment 1, Table 1), the Pt–Pt CN is 5.8 ± 1.3. The corresponding EXAFS data and the theoretical fit are shown in Figure 4a. This CN allows estimation of the nanoparticle size by comparison with model compounds: bulk Pt (CN = 12), a 147-atom cuboctahedron (8.98), and a 309-atom cuboctahedron (9.63).[19] The measured CN is significantly lower than expected for a 240-atom particle (8.98 < CN < 9.63) but is consistent with that previously measured for G6-OH(Pt_{240}) DENs in the solid state (6.1 ± 0.4).[3b] Additionally, the fit reveals a significant contribution from Pt–O (Figure 4b), indicating the presence of unreduced Pt^{2+} surrounded by low-Z neighbors (modeled by oxygen atoms), while the other experiments listed in Table 1 showed little or no contribution from Pt–O. The Pt–O CN for Experiment 1 is also consistent with previous measurements.[3b] Note also that in the presence of multiple X-ray absorption sites (e.g. within the interior and on the surface of the nanoparticle, as in the case here) EXAFS can not discriminate between Pt-O and Pt–N bonds, or between different forms of oxygenated Pt, including Pt–OH_2, Pt–OH, and Pt–O. Very well-defined model structures are required for such discrimination.[20] Additionally, EXAFS measurements do not imply a chemical bond, but simply proximity. Because both the Pt–Pt and Pt–O CNs for Experiment 1 are consistent with previous results for bulk DEN samples, we conclude that there is no significant change induced in the DENs by the immobilization process or the presence of the electrolyte solution.

The EXAFS data for Experiment 2 (Table 1 and Figure 4b), which were obtained with the DEN-modified electrode under potential control (−0.7 V), were somewhat ambiguous as to whether a weak Pt-O contribution (CN = 0.26 ± 0.27) should be included. No Pt–O contribution is included in the fit shown in Figure 4b, but an alternative simulation, which does include this component, is shown in the Supporting Information (Figure S3a). The decision to exclude a contribution from Pt–O is based on the XANES data shown in Figure 5. Figure 5a shows the difference in the white line intensity for a bulk Pt reference foil, a dried powder sample of the unreduced Pt^{2+}/dendrimer complex, and a dried powder sample of the reduced Pt DENs. The presence of oxidized Pt is clearly observed as an increase in the white line intensity of the red spectrum.[21] Figure 5b shows the XANES data for the four experiments summarized in Table 1. Only the spectrum for Experiment 1 reveals this same sort of intensity increase, and therefore a contribution from Pt–O was used to fit just this one EXAFS spectrum.

The EXAFS analysis of Experiment 2 indicates a significantly higher Pt–Pt CN than was measured in Experiment 1 (9.9 ± 1.1

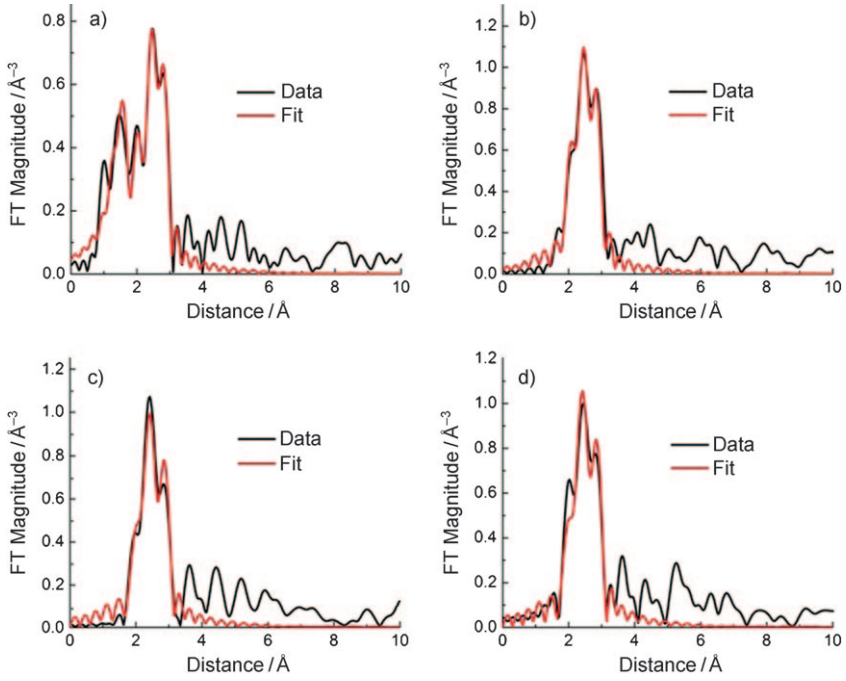

Figure 4. r-space data (black lines) and fitting analysis (red lines) for in situ electrochemical XAFS experiments. The experiments were carried out at fixed potentials using a G6-OH(Pt_{240})-modified carbon cloth working electrode. The electrolyte was 0.1 M $HClO_4$. a) Air-saturated solution at open-circuit potential, b) N_2-saturated solution, E = −0.7 V, c) CO-saturated solution, E = −0.7 V, d) air-saturated solution, open-circuit potential. See Table 1 and the text for a complete summary of the conditions used to obtain these results.

Table 1. Experimental conditions and EXAFS fitting results.

Name	Gas sparge[a]	Potential (vs Hg/Hg_2SO_4)	Pt–Pt CN	Pt–O CN	R_{bkg}
Experiment 1	None	OCP[b]	5.8 ± 1.3	1.6 ± 0.6	1.2
Experiment 2	N_2	−0.7	9.9 ± 1.1	[c]	1.8
Experiment 3	CO	−0.7	10.5 ± 1.5	[d]	1.8
Experiment 4	None	OCP[b]	8.9 ± 0.9	[d]	1.8

[a] This column indicates the gas that was used to sparge the solution during XAFS measurements. For Experiment 1, the solution was air-saturated, but not sparged. For Experiment 4, the solution was sparged with N_2 for 10 min prior to XAFS measurements, but during measurements the cell was open to the atmosphere. [b] Open-circuit potential. [c] A Pt–O contribution was barely detectable but not used for the fit. See text for more information. [d] No Pt–O contribution was included in the fit.

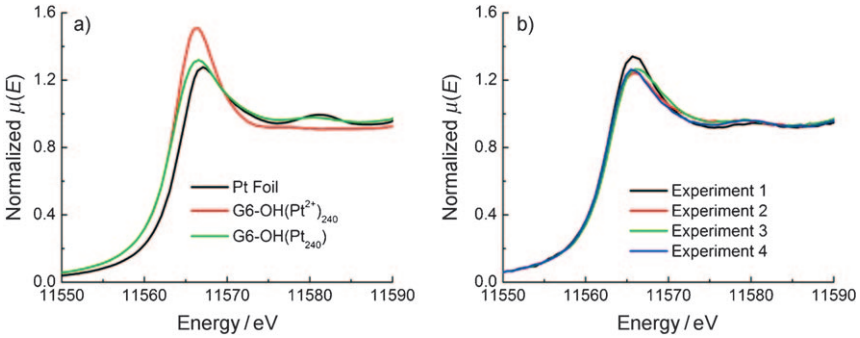

Figure 5. XANES spectra obtained for a) dry, solid-state reference materials and b) the in situ experiments. These experiments were carried out at fixed potentials using a G6-OH(Pt_{240})-modified carbon cloth working electrode. The electrolyte was 0.1 M $HClO_4$. (Black line, Experiment 1): air-saturated solution at open-circuit potential, (red line, Experiment 2): N_2-saturated solution, E = −0.7 V, (green line, Experiment 3): CO-saturated solution, E = −0.7 V, (blue line, Experiment 4) air-saturated solution, open-circuit potential. See Table 1 and the text for a complete summary of the conditions used to obtain these results.

vs 5.8 ± 1.3). Taking into consideration the error in the measurement, this CN is approximately that expected for a 240-atom particle. That is, cuboctahedral nanoparticles containing 147 and 309 atoms have CNs of 8.98 and 9.63, respectively. This result suggests that the application of a sufficiently negative electrode potential (−0.7 V in this case) leads to reduction of Pt^{2+} that was not originally reduced by BH_4^-. This finding is fully consistent with our previously reported model, which suggested that BH_4^- only reduces about 50% of the precursor complexes present in solution.[3b]

Figure 4c shows EXAFS spectra for CO absorbed to the Pt DENs at an electrode potential of −0.7 V (Experiment 3, Table 1). The Pt–Pt CN (10.5 ± 1.5) is about the same as before CO adsorption (9.9 ± 1.1). Additionally, a weak contribution to the EXAFS signal, which is consistent with an interaction between Pt and a low Z element (Figure S3b), was observed. The fitted bond length for this interaction (1.87 ± 0.04 Å) matches that of Pt–CO.[11h,22] While this interaction was not strong enough to be conclusive, we included it in the fit because its presence is anticipated based on the chemistry of the system.

The CO adlayer was removed by scanning the electrode potential twice from −0.7 V to 0.8 V, and then EXAFS data were acquired at open circuit (Experiment 4). The fit of the EXAFS spectrum (Figure 4d) reveals a Pt-Pt CN of 8.9 ± 0.9 (Table 1). This value is a little lower than that measured in the presence of CO but still consistent with a 240 atom nanoparticle.

Our CO adsorption and stripping results are in excellent agreement with those previously reported by Newton et al. for cycling of Pd nanoparticles in CO and NO gas.[23] Specifically, they used a combination of EXAFS and diffuse reflectance infrared spectroscopy, to show that Pd–Pd CNs were higher in the presence of CO. Yevick and Frenkel have recently proposed a quantitative modeling strategy that makes it possible to account for the surface disorder effect on EXAFS results for CNs in strained nanoparticles.[24] They showed that enhanced surface disorder causes a reduction in the apparent metal-metal CN relative to ordered atomic arrangements of the same shape (e.g. in bare clusters vs clusters passivated by H or CO). The Yevick–Frenkel model offers a plausible explanation for the apparent small increase (Table 1) in the Pt–Pt CN in the presence of surface-adsorbed CO. That is, CO may induce additional order in Pt DENs, which results in a more accurate measurement of their CN.

There are two more important findings that result from the EXAFS experiments. First, Pt DENs are fully reduced by application of an appropriate electrode potential. Second, once they are fully reduced, the DENs remain stable during adsorption and subsequent oxidation of CO. That is, it is absolutely clear that surface-immobilized DENs do not aggregate into bulk-like structures (CN = 12) during electrocatalytic oxidation of CO.

2.8. X-ray Photoelectron Spectroscopy (XPS)

The Pt DEN-modified carbon paper was examined by XPS following the XAFS experiments to determine the oxidation state of the nanoparticles. A high-resolution XPS scan of the Pt 4f region of the spectrum, along with relevant peak fitting, is shown in Figure 6. The positions of the main peaks ($Pt\,4f_{5/2}$ = 74.6 eV and $Pt\,4f_{7/2}$ = 71.3 eV) are consistent with our previously reported results for reduced Pt DENs ($Pt\,4f_{7/2}$ = 71.3 eV).[3b] However, the small shoulders apparent at 75.9 and 72.6 eV in Figure 6 indicate the presence of a small amount of oxidized Pt. The full-width at half maximum for the peaks corresponding to fully reduced Pt (green line) is 0.8 eV. However, the peaks corresponding to oxidized Pt (Pt^{x+}, magenta line) are

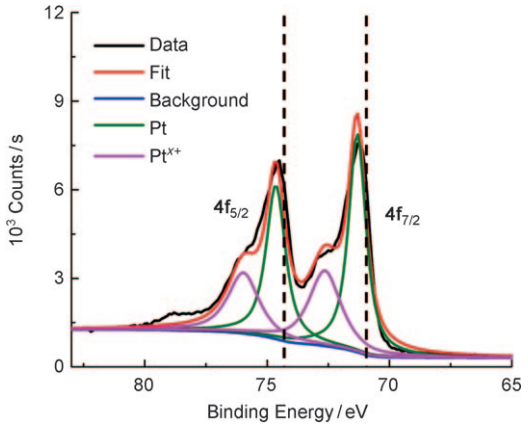

Figure 6. High-resolution XPS spectrum in the Pt4f region for G6-OH(Pt_{240}) DENs. These data were obtained from a section of the electrode used for the XAFS data shown in Figure 4. The dashed lines represent the binding energies for zero-valent Pt ($4f_{7/2}$ = 71.2 eV, $4f_{5/2}$ = 74.5 eV). See text for a discussion of the peak fitting procedure.

much broader: 1.75 eV and 1.40 eV for the $4f_{7/2}$ and $4f_{5/2}$ peaks, respectively. This suggests a distribution of oxidation states. The tail at higher binding energies is likely due to energy losses arising from interactions between photoelectrons and the dendrimer templates. The key point, however, is that all of the XPS data are consistent with the EXAFS results.

3. Summary and Conclusions

We have used in situ electrochemical XAFS to investigate the structural properties of Pt DENs before, during, and after adsorption of CO. The results support our previous finding that reduction of the Pt^{2+}/dendrimer precursor complex with BH_4^- leads to a bimodal distribution of fully reduced and fully unreduced encapsulated Pt structures [i.e. a mixture of G6-OH(Pt_{240}) and G6-OH(Pt^{2+}_{240})].[3b] This distribution is unchanged after passive immobilization of the dendrimers onto the electrode. However, when a negative potential is applied to the carbon-cloth electrode, the CN of the DENs increases from 5.8 to 9.9, indicating complete reduction of the G6-OH(Pt^{2+}_{240} fraction on the electrode and hence conversion of the bimodal distribution to G6-OH(Pt_{240}). Finally, adsorption and desorption of CO onto the Pt DENs do not significantly change the particle structure, but there are some subtle changes that might result from adsorbate-driven ordering of the DENs. The important point, however, is that the presence of the dendrimer hosts stabilize the nanoparticles and prevent agglomeration.

The fact that the structure of DENs is stable on the electrochemical and XAFS time scale (hours) is important, because our objective is to correlate the structure of these materials to their electrocatalytic properties and to first principles calculations. Such correlations require that the size, composition, and structure of nanoparticles be well-defined and not change during the course of catalytic rate measurements. These types of studies are presently underway in our lab, and the results will be reported in due course.

Experimental Section

Chemicals: G6-OH dendrimers were purchased from Dendritech, Inc. (Midland, MI) as 10.0% solutions in methanol. Before use, this solution was dried under vacuum at 22 °C and then reconstituted in sufficient deionized water to make a 100 μM solution. All other chemicals were used as received. K_2PtCl_4 and $NaBH_4$ were purchased from Sigma–Aldrich (Milwaukee, WI). High-purity H_2SO_4 and $HClO_4$ were purchased from J.T. Baker (Phillipsburg, NJ). The carbon paper was AvCarb Grade-P75, purchased from Ballard Material Products (Lowell, MA). Au foil and wire (99.9%) were obtained from Alfa Aesar (Ward Hill, MA). Aqueous solutions were prepared using 18 MΩ·cm Milli-Q water (Millipore, Bedford, MA).

DEN synthesis: DENs consisting of sixth-generation, hydroxyl-terminated PAMAM dendrimers encapsulating Pt nanoparticles containing of an average of 240 atoms [G6-OH(Pt_{240})] were prepared using a previously reported synthesis. Briefly, 240 equiv of Pt^{2+} from a freshly prepared, aqueous 100 mM K_2PtCl_4 solution were added to an aqueous 10.0 μM solution of G6-OH. This solution was stirred for 3.0 days to allow complexation of Pt^{2+} to tertiary amines within the dendrimer.[3b] This G6-OH(Pt^{2+}_{240} complex was reduced for 24.0 h in a tightly sealed vial using a ~ten-fold molar excess of freshly prepared, aqueous 0.50 M $NaBH_4$. Finally, the DENs solution was dialyzed for 24.0 h into 4.0 L of Milli-Q water using a 12 kDa cutoff dialysis sack (Sigma–Aldrich).

Characterization: UV-vis absorption spectra were acquired using a Hewlett–Packard HP8453 spectrometer and quartz cuvettes having a pathlength of 0.10 cm. A 10.0 μM aqueous G6-OH solution was used for background subtraction.

Transmission electron microscopy (TEM) was carried out using a JEOL-2010F TEM operating at 200 kV. Samples were prepared by dropping the appropriate solution onto a 20 nm-thick, carbon-coated, 400-mesh Cu grid (EM Sciences, Gibbstown, NJ) supported on filter paper, and then drying in air. X-ray photoelectron spectroscopy (XPS) data were obtained using a Kratos Axis Ultra DLD spectrometer having a monochromatic Al Kα X-ray source. High-resolution spectra were collected at a pass energy of 20 eV, a resolution of 0.1 eV, and a dwell time of 1.00 s. Survey scans were collected at a pass energy of 160 eV, a resolution of 1 eV, and a dwell time of 1.00 s. XPS samples were cut from the carbon paper used for the EXAFS measurements. To account for sample charging, the recorded binding energies were adjusted so that the energy of the carbon peak matched the previously measured value for the dendrimer (286.0 eV).[3b] Peak fitting was performed using XPSPEAK software. Both the separation and the ratio of areas for the Pt $4f_{7/2}$ and $4f_{5/2}$ peaks were constrained to be equal for both the reduced and oxidized Pt species. A Shirley background was used while the peaks were 80% Lorentzian-20% Gaussian.

XAFS spectra were obtained at beamline X18B of the National Synchrotron Light Source at the Brookhaven National Laboratory using a custom-designed cell. More information about the cell is provided later in this section, in the main text, and in the Supporting Information. The DENs were immobilized onto the working electrode by soaking electrochemically activated carbon paper (vide infra) overnight in a dialyzed, aqueous solution of Pt DENs. Once modified with DENs, the electrodes were rinsed and kept wet until use. All XAFS data were obtained in fluorescence mode using a Lytle detector, Soller slits, and a Ge filter. A reference Pt foil was measured between successive samples and used for energy calibration and alignment. As many as 10 EXAFS scans of the Pt adsorption edge were collected and averaged to improve the signal-to-noise ratio.

The data were processed using the Athena program and fit using the FEFF6 theory and the Artemis program.[10,25] The fitting model was constructed using four variables (CN, Δr, ΔE_0, and σ^2) for each interaction (Pt–Pt, Pt–O, or Pt–C). The value of S_O^2 (0.84) was fixed to that of a Pt foil measured on the same beamline. The foil was fit over four shells to a perfect fcc lattice to obtain S_O^2. A typical analysis fit either four or eight variables to the data which contained ten independent data points. The initial choice of R_{bkg}, a background subtraction factor, was made during the data processing and finalized during the analysis stage due to the difficulty of correctly determining this parameter in the case of low Z absorbers. Fine tuning of its value was made by visual examination of the fit quality and inspection of the quantitative goodness of the fit; that is, the reduced χ^2 and *R*-factor reported by Artemis.

Electrochemical cells: Three distinct types of electrochemical cells were used in this work. Photographs of each cell are provided in the Supporting Information (Figure S4). The first type of cell used is referred to as the "standard electrochemical cell" (Figure S4a). This cell is a cylindrical glass container, open at the top, and it has a volume of 20 mL. All three electrodes are inserted into the cell from the top. When a carbon paper electrode is used in this cell, a large area of the electrode is exposed to the electrolyte solution. However, the active electrochemical area is limited to that which has been rendered hydrophilic by electrochemical pretreatment. The electrochemical cell used to make the carbon paper hydrophilic is referred to as the "Teflon cell," and it is illustrated schematically in Figure S5 and a photograph is provided in Figure S4b. This cell defines a geometric area of 3.1 cm^2 on the carbon paper working electrode.

The final electrochemical cell is referred to as the "XAFS cell", and it is shown in Figure S4c and illustrated in Scheme 1. This cell was used for all in situ XAFS experiments. Alternative designs have been used by other groups.[11g,i,26] As shown in Scheme 1, our cell design balances the requirements for electrochemical and XAFS measurements. In addition, this design provides for continuous gas sparging during the XAFS experiments without bubbles forming either on the electrode or near the XAFS window.

Electrochemistry: Unless specified otherwise, all electrochemistry experiments employed a Hg/Hg_2SO_4 reference electrode (CH Instruments, Austin, TX) and a glassy carbon counter electrode. All potentials are reported vs the Hg/Hg_2SO_4 reference electrode. The standard electrochemical cell was used for experiments employing either the glassy carbon working electrode (GCE) or the Pt working electrode, as well as for CO oxidation scans using the carbon paper working electrode. Carbon paper pretreatment, cleaning scans, and H-adsorption experiments were performed in the Teflon cell.

Immobilization of Pt DENs on the GCE followed a previously reported procedure.[3d,e,4] Briefly, The GCE was polished with 0.3 μm alumina, rinsed, dried with N_2, and then immersed in a cell containing 0.1 M $LiClO_4$, the dialyzed DENs solution, a Pt wire counter electrode, and a Hg/Hg_2SO_4 reference electrode. During immobilization, the electrode potential was scanned from −0.2 to 0.7 V at 10 $mV\,s^{-1}$ for three cycles. For the oxidation of CO in the standard cell, the working electrode (either a macroscopic Pt electrode, a Pt DENs-modified GCE, or a Pt DENs-modified carbon paper electrode) was first placed in a CO-saturated, 0.1 M $HClO_4$ solution. The potential of this electrode was stepped to −0.7 V and held there for 10 min. Next, N_2 was bubbled into the solution for 10 additional minutes while maintaining the electrode at −0.7 V. The electrode was then swept from −0.7 V to 0.8 V at 50 $mV\,s^{-1}$ for two full cycles.

Electrochemical pretreatment of the carbon cloth, necessary to render it hydrophilic, followed a procedure previously reported by Godinez and coworkers.[17] Specifically, the potential of the carbon cloth was scanned 4 times between 1.0 V and −1.0 V at 100 $mV\,s^{-1}$ in an aqueous 0.5 M H_2SO_4 electrolyte solution. These scans started and ended at 0.0 V, and the initial scan direction was negative. Additional information about the pretreatment procedure is provided in the Supporting Information (Figure S6).

Following DEN immobilization, nanoparticle cleaning scans were performed by cycling the potential of the carbon cloth 10 times between 0.185 V and −0.715 V at 50 $mV\,s^{-1}$ in an aqueous 0.1 M $HClO_4$ electrolyte solution. These scans started and ended at 0.0 V, and the initial scan direction was negative. Voltammetry in the hydrogen adsorption region was performed immediately following the cleaning scans. In this case, the scan rate was 50 $mV\,s^{-1}$ and three cycles were recorded.

In situ XAFS experiments were carried out in 0.1 M $HClO_4$ aqueous solutions, saturated with either N_2 or CO, using the XAFS cell. The electrolyte solutions were sparged with the appropriate gas for at least 10 min before placing the working electrode under potential control, and, unless otherwise specified, sparging continued throughout the time required to obtain XAFS spectra. The in situ CO experiments started with a linear sweep from −0.2 V to −0.7 V at 10 $mV\,s^{-1}$, and then the potential was held at −0.7 V for the duration of the XAFS measurements. The cell was then purged with N_2 for 10 min to remove residual CO from the solution. Adsorbed CO was oxidized by cycling the potential twice from −0.7 V to 0.8 V at 50 $mV\,s^{-1}$ with no gas flowing. These scans began and ended at −0.7 V. The final XAFS spectrum was obtained at the open circuit potential (OCP) with no gas flowing.

Acknowledgements

MGW, VSM, and RMC gratefully acknowledge financial support from the U.S. Department of Energy Office of Basic Energy Sciences (Grant No. DE-FG02-09ER16090). RMC acknowledges sustained support from the Robert A. Welch Foundation (Grant F-0032). AIF acknowledges support of the Department of Energy Grant No. DE-FG02-03ER15476. Use of the NSLS was supported by the U.S. Department of Energy, Office of Science, Office of Basic Energy Sciences, under Contract No. DE-AC02-98CH10886. Beamline X18B at the NSLS is supported in part by the Synchrotron Catalysis Consortium, U. S. Department of Energy Grant No. DE-FG02-05ER15688.

Keywords: catalysis · electrochemistry · nanoparticles · platinum · XAFS spectroscopy

[1] a) P. K. Jain, X. Huang, I. H. El-Sayed, M. A. El-Sayed, *Acc. Chem. Res.* **2008**, *41*, 1578; b) R. W. Murray, *Chem. Rev.* **2008**, *108*, 2688.
[2] W. J. Tang, G. Henkelman, *J. Chem. Phys.* **2009**, *130*, 194504.
[3] a) O. S. Alexeev, A. Siani, G. Lafaye, C. T. Williams, H. J. Ploehn, M. D. Amiridis, *J. Phys. Chem. B* **2006**, *110*, 24903; b) M. R. Knecht, M. G. Weir, V. S. Myers, W. D. Pyrz, H. Ye, V. Petkov, D. J. Buttrey, A. I. Frenkel, R. M. Crooks, *Chem. Mater.* **2008**, *20*, 5218; c) R. W. J. Scott, O. M. Wilson, R. M. Crooks, *J. Phys. Chem. B* **2005**, *109*, 692; d) H. Ye, J. A. Crooks, R. M. Crooks, *Langmuir* **2007**, *23*, 11901; e) H. Ye, R. M. Crooks, *J. Am. Chem. Soc.* **2005**, *127*, 4930.
[4] H. Ye, R. M. Crooks, *J. Am. Chem. Soc.* **2007**, *129*, 3627.
[5] a) G. Vijayaraghavan, K. J. Stevenson, *Langmuir* **2007**, *23*, 5279; b) S. S. Mark, M. Bergkvist, X. Yang, E. R. Angert, C. A. Batt, *Biomacromolecules* **2006**, *7*, 1884; c) A. Singh, B. D. Chandler, *Langmuir* **2005**, *21*, 10776;

d) Y. Gu, H. Xie, J. Gao, D. Liu, C. T. Williams, C. J. Murphy, H. J. Ploehn, *Langmuir* **2005**, *21*, 3122; e) P. J. Pellechia, J. Gao, Y. Gu, H. J. Ploehn, C. J. Murphy, *Inorg. Chem.* **2004**, *43*, 1421; f) F. Tarazona-Vasquez, P. B. Balbuena, *J. Phys. Chem. A* **2007**, *111*, 945; g) F. Tarazona-Vasquez, P. B. Balbuena, *J. Phys. Chem. A* **2007**, *111*, 932; h) D. Yamamoto, S. Watanabe, M. T. Miyahara, *Langmuir* **2010**, *26*, 2339.

[6] K. Yamamoto, T. Imaoka, W.-J. Chun, O. Enoki, H. Katoh, M. Takenaga, A. Sonoi, *Nat. Chem.* **2009**, *1*, 397.

[7] a) M. Arenz, K. J. J. Mayrhofer, V. Stamenkovic, B. B. Blizanac, T. Tomoyuki, P. N. Ross, N. N. Markovic, *J. Am. Chem. Soc.* **2005**, *127*, 6819; b) S. Gilman, *J. Phys. Chem.* **1962**, *66*, 2657; c) F. Maillard, M. Eikerling, O. V. Cherstiouk, S. Schreier, E. R. Savinova, U. Stimming, *Faraday Discuss.* **2004**, *125*, 357; d) K. J. J. Mayrhofer, B. B. Blizanac, M. Arenz, V. Stamenkovic, P. N. Ross, N. N. Markovic, *J. Phys. Chem. B* **2005**, *109*, 14433.

[8] K. J. Andersson, F. Calle-Vallejo, J. Rossmeisl, I. Chorkendorff, *J. Am. Chem. Soc.* **2009**, *131*, 2404.

[9] F. Maillard, S. Schreier, M. Hanzlik, E. R. Savinova, S. Weinkauf, U. Stimming, *Phys. Chem. Chem. Phys.* **2005**, *7*, 385.

[10] M. Newville, *J. Synchrotron Radiat.* **2001**, *8*, 322.

[11] a) J. McBreen, S. Mukerjee, *J. Electrochem. Soc.* **1995**, *142*, 3399; b) S. Mukerjee, J. McBreen, *J. Electrochem. Soc.* **1999**, *146*, 600; c) S. Mukerjee, R. C. Urian, S. J. Lee, E. A. Ticianelli, J. McBreen, *J. Electrochem. Soc.* **2004**, *151*, A1094; d) A. Rose, E. M. Crabb, Y. Qian, M. K. Ravikumar, P. P. Wells, R. J. K. Wiltshire, J. Yao, R. Bilsborrow, F. Mosselmans, A. E. Russell, *Electrochim. Acta* **2007**, *52*, 5556; e) A. E. Russell, S. Maniguet, R. J. Mathew, J. Yao, M. A. Roberts, D. Thompsett, *J. Power Sources* **2001**, *96*, 226; f) A. E. Russell, A. Rose, *Chem. Rev.* **2004**, *104*, 4613; g) R. J. K. Wiltshire, C. R. King, A. Rose, P. P. Wells, M. P. Hogarth, D. Thompsett, A. E. Russell, *Electrochim. Acta* **2005**, *50*, 5208; h) S. Maniguet, R. J. Mathew, A. E. Russell, *J. Phys. Chem. B* **2000**, *104*, 1998; i) J. McBreen, W. E. O'Grady, K. I. Pandya, R. W. Hoffman, D. E. Sayers, *Langmuir* **1987**, *3*, 428; j) S. Mukerjee, S. Srinivasan, M. P. Soriaga, J. McBreen, *J. Electrochem. Soc.* **1995**, *142*, 1409; k) C. Roth, N. Benker, T. Buhrmester, M. Mazurek, M. Loster, H. Fuess, D. C. Koningsberger, D. E. Ramaker, *J. Am. Chem. Soc.* **2005**, *127*, 14607; l) K. Sasaki, L. Zhang, R. R. Adzic, *Phys. Chem. Chem. Phys.* **2008**, *10*, 159; m) F. J. Scott, S. Mukerjee, D. E. Ramaker, *J. Electrochem. Soc.* **2007**, *154*, A396; n) F. J. Scott, C. Roth, D. E. Ramaker, *J. Phys. Chem. C* **2007**, *111*, 11403; o) M. Teliska, W. E. O'Grady, D. E. Ramaker, *J. Phys. Chem. B* **2004**, *108*, 2333; p) M. Teliska, W. E. O'Grady, D. E. Ramaker, *J. Phys. Chem. B* **2005**, *109*, 8076.

[12] E. I. Santiago, M. J. Giz, E. A. Ticianelli, *J. Solid State Electrochem.* **2003**, *7*, 607.

[13] K. J. J. Mayrhofer, M. Arenz, B. B. Blizanac, V. Stamenkovic, P. N. Ross, N. M. Markovic, *Electrochim. Acta* **2005**, *50*, 5144.

[14] a) D. Armand, J. Clavilier, *J. Electroanal. Chem.* **1989**, *270*, 331; b) A. Rodes, J. Clavilier, J. M. Orts, J. M. Feliu, A. Aldaz, *J. Electroanal. Chem.* **1992**, *338*, 317; c) S. Taguchi, A. Aramata, *J. Electroanal. Chem.* **1998**, *457*, 73.

[15] O. V. Cherstiouk, P. A. Simonov, V. I. Zaikovskii, E. R. Savinova, *J. Electroanal. Chem.* **2003**, *554–555*, 241.

[16] a) A. J. Bard, L. R. Faulkner, *Electrochemical Methods: Fundamentals and Applications*, 2nd ed., John Wiley & Sons, Inc., Hoboken, NJ, **2001**;b) E. Aschauer, R. Fasching, M. Varahram, G. Jobst, G. Urban, G. Nicolussi, W. Husinsky, G. Friedbacher, M. Grasserbauer, *J. Electroanal. Chem.* **1997**, *426*, 157; c) D. Gilroy, B. E. Conway, *Can. J. Chem.* **1968**, *46*, 875.

[17] J. Ledesma-García, I. L. E. García, F. J. Rodríguez, T. W. Chapman, L. A. Godínez, *J. Appl. Electrochem.* **2008**, *38*, 515.

[18] R. L. McCreery, in *Electroanalytical Chemistry: A Series of Advances Vol. 17* (Ed.: A. J. Bard), Marcel Dekker, New York, **1991**, pp. 221.

[19] a) D. Glasner, A. I. Frenkel, in *XAFS 13 Proc. Int. Conf. X-ray Absorpt. Fine Struct. Vol. 882* (Eds.: B. Hedman, P. Painetta), Amer Inst Physics, Melville, **2007**, pp. 746;b) A. Jentys, *Phys. Chem. Chem. Phys.* **1999**, *1*, 4059.

[20] E. Poverenov, I. Efremenko, A. I. Frenkel, Y. Ben-David, L. J. W. Shimon, G. Leitus, J. M. L. Marin, D. Milstein, *Nature* **2008**, *455*, 1093.

[21] H. Yoshida, S. Nonoyama, Y. Yazawa, T. Hattori, *Phys. Scripta* **2005**, *T115*, 813.

[22] a) D. F. Ogletree, M. A. Van Hove, G. A. Somorjai, *Surf. Sci.* **1986**, *173*, 351; b) X. Zhou, G. Zhuang, Y. Chen, S. A. Kellar, E. J. Moler, Z. Hussain, D. A. Shirley *Vol. 2009*, **1998**.

[23] M. A. Newton, C. Belver-Coldeira, A. Martinez-Arias, M. Fernandez-Garcia, *Nat. Mater.* **2007**, *6*, 528.

[24] A. Yevick, A. I. Frenkel, *Phys. Rev. B* **2010**, *81*, 115451.

[25] a) B. Ravel, M. Newville, *J. Synchrotron Radiat.* **2005**, *12*, 537; b) J. J. Rehr, R. C. Albers, *Rev. Mod. Phys.* **2000**, *72*, 621.

[26] I. V. Malakhov, S. G. Nikitenko, E. R. Savinova, D. I. Kochubey, N. Alonso-Vante, *Nucl. Instrum. Meth. A* **2000**, *448*, 323.

Received: June 5, 2010
Published online on August 16, 2010

